2016 American Control Conference (ACC)
Boston Marriott Copley Place
July 6-8, 2016. Boston, MA, USA

Visual Servoing of an Inverted Pendulum on Cart using a Mounted Smartphone

Anthony Brill[1], Jared A. Frank[1], and Vikram Kapila[1]

Abstract— **Over the last several decades, visual servoing–a vision-based control approach–has been explored as a popular and inexpensive contactless measurement alternative for a variety of industrial robotic systems. Moreover, recent years have witnessed rapid advancements in mobile device applications that have pushed the envelope in the capabilities of smartphone cameras. In this paper, an eye-in-hand pose-based visual servoing (PBVS) approach is presented wherein a smartphone mounted to an inverted pendulum on cart (IPC) system measures both the translational position of a motorized cart and the angular orientation of a pendulum arm for the purpose of feedback control. To perform vision-based control of the IPC system, a discrete-time linear quadratic gaussian (LQG) controller is implemented. Experimental results are presented to characterize the relationships between the frame rate and image resolution of the smartphone camera, processing and wireless communication delays, the measurement noise, and the performance of the closed-loop system.**

I. Introduction

The increasing popularity of smartphones has led to a new age of personal computing, where the ability to sense, process, and communicate information is available within an arm's reach. Today's smartphones are equipped with powerful embedded sensors (e.g., accelerometer, gyroscope, GPS, and camera), offering a diverse array of mobile sensing opportunities. Specifically, the on-board cameras are one of the most powerful measurement tools currently available on these mobile devices, and have been used for everything from entertainment to assisting the visually impaired [14].

The sensing capabilities of smartphones have already been used to teach physics concepts such as the relationship between angular velocity and centripetal acceleration [11] and the rotational energy in a pendulum [10]. Students have also benefited from interactions with smart mobile devices while performing laboratory experiments [5]. The ubiquity of smartphones introduces unique opportunities for students to integrate their personal devices directly into physical systems to provide sensing, storage, processing, and communication. Furthermore, mounted smartphones can provide readily-accessible, inquiry-based learning experiences with test-beds.

Visual servoing allows data obtained with visual sensors to be used in the feedback control of a physical system. Visual servoing can be implemented in either an image-based (IBVS), pose-based (PBVS), or hybrid approach. To calculate control actions, IBVS approaches make use of the error between estimated and desired locations of features in image coordinates, while PBVS estimates the transformation between a real-world coordinate system and the camera coordinate system. IBVS methods have been used to stabilize a number of physical systems, such as IPC test-beds [4], [15], however no implementation of PBVS has been found to address the IPC problem. The implementation of visual servoing can follow either an eye-in-hand or eye-to-hand paradigm [3], [8]. Eye-in-hand involves mounting the camera to the system being controlled, while eye-to-hand involves pointing the camera at the system, often with the camera fixed in the environment. The more traditional eye-to-hand approach has been thoroughly explored in the stabilization of IPC system [4]. Prior research has also considered the eye-in-hand configuration to stabilize a wheeled inverted pendulum, however the use of vision has been limited to measuring the linear displacement and not the rotational degree of freedom [7].

Fig. 1: A smartphone-mounted IPC system.

The classical IPC test-bed has been extensively employed to investigate a variety of control methods and their technological implementations. Moreover, as seen above, vision-based methods are being widely explored for control applications, including the IPC. However, no implementations have been found that employ pose estimates or cameras mounted on the test-bed for the IPC system. Thus, in this paper, a PBVS approach with an eye-in-hand configuration is explored to stabilize an IPC system using a mounted smartphone (see Figure 1). The IPC test-bed's inherent nonlinearities, underactuation, large bandwidth, and open-loop instability impose demands on processing time, frame rate, and image quality when using vision-based approaches [9]. This paper examines the feasibility of smartphone-mounted control test-beds and the effects of the aforementioned parameters on the stability and performance of the closed-loop. In Section II, an overview of the system and user interface are presented. Section III describes the image processing algorithm executed on the mobile application to

This work is supported in part by the National Science Foundation awards RET Site EEC-1132482, GK-12 Fellows DGE: 0741714, and DRK-12 DRL: 1417769, and NY Space Grant Consortium grant 76156-10488.

[1]Mechatronics and Controls Lab, Mechanical and Aerospace Engineering, NYU Tandon School of Engineering, Brooklyn, NY 11201 [brill.anthony, jared.alan, vkapila]@nyu.edu

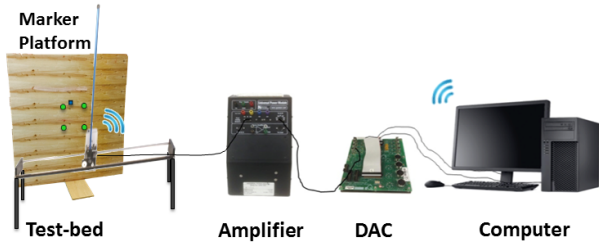

Fig. 2: Schematic of the IPC with mounted smartphone.

obtain vision-based measurements of both the position of the motorized cart and angular position of the pendulum arm. Section IV discusses the linearized sampled-data model of the IPC system used to design an LQG controller for stabilizing the test-bed. Section V presents the results of the experiment conducted with the IPC system mounted with the smartphone to investigate the relationships between the frame rate and image resolution of the smartphone camera, the processing and wireless communication delays, the measurement noise, and the performance of the closed-loop system. Section VI offers some concluding remarks.

II. System Description

The system used in this study is an IPC test-bed [1] with a smartphone mounted to the rotational axis of a 60.6 cm long pendulum arm. The motorized cart is driven using a power amplifier that receives control signals from a personal computer (PC) via a data acquisition and control board. The mounted smartphone is responsible for all sensing on the system. The mobile application running on the smartphone uses visual observations of an object in the environment to obtain the linear and rotational position estimates of the state of the smartphone (and thus the IPC). Measurements are transmitted over a Wi-Fi network to the PC, which computes and relays control signals to the test-bed using the MATLAB/Simulink environment. The components of the proposed system are shown in Figure 2. The smartphone used in this study is an Apple iPhone 6 Plus, which has a 5.5 inch (140 mm), 1080×1920 pixel multi-touch display, 1.4 GHz dual-core processor, and a 1.2-megapixel front-facing camera. These embedded technologies allow the smartphone to provide on-board sensing, storage, computation, and communication to the IPC system.

The front-facing camera of the iPhone 6 Plus supports frame rates up to 60 frames per second (fps) and resolutions as low as 192×144 pixels. In front of the IPC test-bed, and in view of the camera, a planar object is fitted with five colored markers. An image processing algorithm, running in the background of a mobile application, is used to extract the 3D pose of the marker platform with respect to the translating and rotating camera of the iPhone. Since the smartphone is rigidly mounted to the test-bed, the pose of the object can be used to determine both the position of the motorized cart and the angular position of the pendulum arm.

Attaching the smartphone to the IPC test-bed not only allows for the on-board sensor feedback of the phone to be used for control, but it also allows for the design of

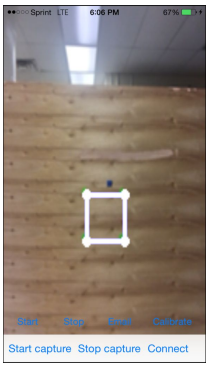

Fig. 3: Screenshot of the user interface.

an interactive user interface that is mounted to the experiment. The mobile application developed for this experiment allows users to wirelessly connect to the PC, start and stop video capture, calibrate sensor measurements, and collect experimental data that users can email to themselves or to collaborators for further analysis. The touch screen display provides useful visual feedback to the user regarding the data collected by the application and the status of the image processing algorithm used to estimate the state of the IPC system. This allows users to easily calibrate and troubleshoot the system. A screenshot of the mobile application running on the iPhone 6 Plus is shown in Figure 3.

III. Computer Vision

Rigidly mounting the smartphone to the IPC system, as shown in Figure 1, allows for the vision-based estimation of the 3D pose of an object observed in the environment with respect to the smartphone's camera. Marker-based techniques are used to compute and map this pose to the linear displacement of the cart and angular orientation of the pendulum arm.

A. Marker Detection and Association

Vision-based pose estimation of a planar object in front of the IPC test-bed is facilitated by attaching bright colored markers to the object. The planar object is located such that the smartphone camera can observe it in the environment from all possible states of the IPC system. The markers have known locations in the world coordinate system. The locations of their centers in image coordinates are detected using a color segmentation approach involving thresholding in the hue-saturation-value (HSV) space and morphological filtering operations to remove small amounts of noise [6].

Real-time constraints on the stability of the closed-loop feedback control system demand an efficient implementation of the computer vision algorithm to reduce latency in data collection. To improve the efficiency of computation of vision-based data on the smartphone and to maximize the frame rate, regions of interest are incorporated into the image processing algorithm [6] and image resolution is reduced to the lowest quality available (192×144). However, decrease in image resolution produces significant increase in noise for measurements extracted from the vision data. This problem is further discussed in Section V.

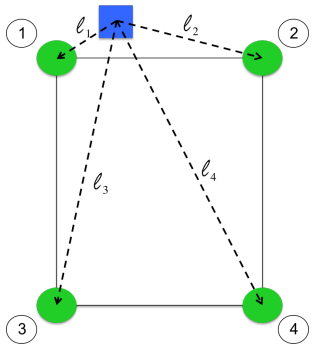

Fig. 4: Diagram of markers placed on the planar object in front of the IPC test-bed such that $l_1 < l_2 < l_3 < l_4$.

On the planar object, four green markers and one blue marker are positioned in a geometric configuration wherein each green marker is identified by its relative position from the blue marker (see Figure 4). In order for the object pose to be estimated correctly, the identity of each green marker can not change between frames. Since $l_1 << l_2$, $l_2 << l_3, l_4$, markers 1 and 2 are always detected correctly. Next, to ensure that markers 3 and 4 are sorted correctly, two line segments are created in the image plane–one between the image coordinates of markers 1 and 4 and the other between the image coordinates of markers 2 and 3. If the line segments intersect, the markers are deemed to have been sorted successfully, otherwise markers 3 and 4 are switched.

B. 3D Pose Estimation and Measurements

To obtain vision-based measurements of the position of the motorized cart and angular position of the pendulum, the pose of an object coordinate system attached to the first green marker is estimated with respect to the camera coordinate system. This transformation consists of a rotation matrix and a translation vector. After the smartphone camera has been calibrated [16] and the location of each marker has been given in world coordinates, the 2D-3D point correspondence problem is solved [2]. In this way, the angle of the pendulum arm about its rotational axis can be found as the negative of the orientation between the marker coordinate system and camera coordinate system. The position of the cart is measured as the component of translation between the camera and the marker coordinate systems in the direction along the cart's track. Since the pendulum is assumed to exhibit only small angular deviations from equilibrium, the displacement of the cart is equated with the distance between the origin of the marker coordinate system and the camera coordinate system in the camera coordinate system.

IV. Modeling and Control

To implement a system in which the IPC test-bed is stabilized using visual feedback from a mounted smartphone, a discretized model is used to design an LQG controller.

A. Plant Model

A diagram of the IPC system is shown in Figure 5. The IPC system consists of a pendulum arm mounted to a cart that translates on a linear track. The control objective is to

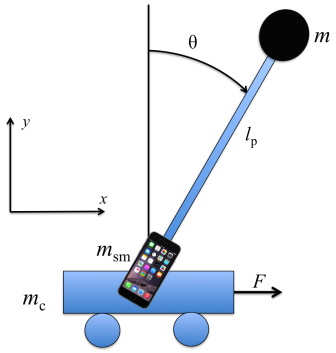

Fig. 5: Model of the smartphone-mounted IPC system.

stabilize the pendulum arm in the upright orientation and keep the cart on the center of the track, using measurements of the cart position and pendulum arm orientation. The cart is at a distance x in meters from the center position on the track and the pendulum arm is rotated from its upright orientation by an angle θ in radians. In this system, friction between various interacting surfaces is assumed to be negligible. The equations of motion for this conservative system can be derived using the Newton's method or the Euler-Lagrange approach outlined in [1], [13], with the mass of the smartphone, m_{sm}, and its moment of inertia about the rotational axis, $J_{\text{sm}} \triangleq m_{\text{sm}}(l_{\text{sm}}^2 + w_{\text{sm}}^2)/12$, added to the equations, where l_{sm} and w_{sm} are the length and width of the smartphone, respectively. Thus,

$$(m+M)\ddot{x} + m\ddot{\theta} l_{\text{p}} \cos\theta - m\dot{\theta}^2 l_{\text{p}} \sin\theta = F, \quad (1)$$

$$ml_{\text{p}} \cos\theta \ddot{x} - ml_{\text{p}} \sin\theta \dot{\theta}\dot{x} + (ml_{\text{p}}^2 + J_{\text{sm}})\ddot{\theta} - mgl_{\text{p}} \sin\theta = 0, \quad (2)$$

where m is the mass of the pendulum arm, $M \triangleq m_{\text{c}} + m_{\text{sm}}$ is the sum of the mass of the cart and mass of the smartphone, and l_{p} is the half-length of the pendulum arm. Note that F is the translational force generated by a DC motor driving the cart, and as delineated below, F is related to the applied voltage V and rotational velocity of the motor shaft (equivalently, cart translational velocity $\dot{x}$) [1]

$$F(t) = \frac{K_{\text{m}} K_{\text{g}}}{Rr} V(t) - \frac{K_{\text{m}}^2 K_{\text{g}}^2}{Rr^2} \dot{x}(t), \quad (3)$$

where K_{m} is the motor-torque constant, K_{g} is the gear ratio, R is the electrical resistance of the motor, and r is the radius of the wheel of the cart. Next, linearizing (1), (2) by assuming small angle θ and neglecting nonlinear effects yields

$$(m+M)\ddot{x}(t) + ml_{\text{p}}\ddot{\theta}(t) = F(t), \quad (4)$$

$$ml_{\text{p}}\ddot{x}(t) + (ml_{\text{p}}^2 + J_{\text{sm}})\ddot{\theta}(t) - mgl_{\text{p}}\theta(t) = 0. \quad (5)$$

Solving for $\ddot{x}$ and $\ddot{\theta}$ and choosing state variables $\mathbf{x}(t) \triangleq [x(t) \quad \theta(t) \quad \dot{x}(t) \quad \dot{\theta}(t)]^{\text{T}}$, the IPC system of (4), (5) yields the following state-space model

$$\dot{\mathbf{x}}(t) = A_1 \mathbf{x}(t) + B_1 F(t), \quad (6)$$

$$A_1 \triangleq \begin{bmatrix} 0 & 0 & 1 & 0 \\ 0 & 0 & 0 & 1 \\ 0 & -\frac{mgl_{\text{p}}}{J_{\text{eq}}\gamma} & 0 & 0 \\ 0 & \frac{(M+m)g}{J_{\text{eq}}\gamma} & 0 & 0 \end{bmatrix}, \quad B_1 \triangleq \begin{bmatrix} 0 \\ 0 \\ \frac{1}{ml_{\text{p}}\gamma} \\ -\frac{1}{J_{\text{eq}}\gamma} \end{bmatrix},$$

where $\gamma \triangleq \frac{m+M}{ml_{\rm p}} - \frac{ml_{\rm p}}{J_{\rm eq}}$ and $J_{\rm eq} \triangleq J_{\rm sm} + ml_{\rm p}^2$. Next, using (3) for the force $F(t)$ in (6) yields the state-space representation

$$\dot{\mathbf{x}}(t) = A\mathbf{x}(t) + BV(t), \quad y(t) = C\mathbf{x}(t), \tag{7}$$

$$A \triangleq \begin{bmatrix} 0 & 0 & 1 & 0 \\ 0 & 0 & 0 & 1 \\ 0 & -\frac{mgl_{\rm p}}{J_{\rm eq}\gamma} & -\frac{1}{ml_{\rm p}\gamma}\left(\frac{K_{\rm m}^2K_{\rm g}^2}{Rr^2}\right) & 0 \\ 0 & \frac{(M+m)g}{J_{\rm eq}\gamma} & \frac{1}{J_{\rm eq}\gamma}\left(\frac{K_{\rm m}^2K_{\rm g}^2}{Rr^2}\right) & 0 \end{bmatrix},$$

$$B \triangleq \begin{bmatrix} 0 \\ 0 \\ \frac{1}{ml_{\rm p}\gamma}\left(\frac{K_{\rm m}K_{\rm g}}{Rr}\right) \\ -\frac{1}{J_{\rm eq}\gamma}\left(\frac{K_{\rm m}K_{\rm g}}{Rr}\right) \end{bmatrix}, \quad C \triangleq \begin{bmatrix} 1 & 0 & 0 & 0 \\ 0 & 1 & 0 & 0 \end{bmatrix},$$

where $y(t)$ denotes the measured output.

The numerical values for physical parameters of our laboratory IPC system are provided in Table I below.

TABLE I: Values for physical parameters of the IPC system.

Physical quantity	Symbol	Numerical value	Units
Cart mass	$m_{\rm c}$	0.815	kg
Pendulum mass	m	0.210	kg
Smartphone mass	$m_{\rm sm}$	0.172	kg
Pendulum length	$2l_{\rm p}$	2×0.303	m
Cart wheel radius	r	0.0254/4	m
Smartphone length	$l_{\rm sm}$	0.1581	m
Smartphone width	$w_{\rm sm}$	0.0778	m
Gravitational constant	g	9.8	m/s^2
DC-motor resistance	R	2.6	Ω
Motor constant	$K_{\rm m}$	0.00767	
Gear ratio	$K_{\rm g}$	3.7	

B. Discretization

For the design of a discrete-time LQG controller, the state-space model of (7) is discretized at each sampling instant kT, $k = 0, 1, 2, \ldots$, to yield

$$\mathbf{x}[(k+1)T] = \Phi\mathbf{x}[kT] + \Theta u[kT], \tag{8}$$

$$y[kT] = C\mathbf{x}[kT], \tag{9}$$

where $\Phi \triangleq e^{AT}$ is the state transition matrix of the model and $\Theta \triangleq \int_0^T e^{A(T-\tau)}Bd\tau$. Before designing the LQG controller (equivalently, the design of Kalman filter gain and linear quadratic regulator gain) for the above sampled-data model with sampling time T, the observability and controllability of the system are verified by confirming that the following observability matrix, M_o, and controllability matrix, M_c, are of full rank

$$M_o = \begin{bmatrix} C \\ C\Phi \\ C\Phi^2 \\ C\Phi^3 \end{bmatrix}, \quad M_c = \begin{bmatrix} \Theta \\ \Phi\Theta \\ \Phi^2\Theta \\ \Phi^3\Theta \end{bmatrix}^{\rm T}.$$

C. State Estimation

The proposed computer vision approach provides measurements y of only two of the states needed for full-state feedback control. These measurements will contain noise, due to factors such as imperfections in image quality, scene illumination, and the color segmentation procedure. Noise associated with the detected centers of the markers will result in noisy cart position and pendulum angle measurements. Therefore, a steady-state discrete-time Kalman filter is used to obtain estimates $\hat{\mathbf{x}}(k{\rm T})$ of the discretized state $\mathbf{x}(k{\rm T})$, which includes two measured states (i.e., the cart position and the pendulum angle) and two unmeasured states (i.e., the velocity of the cart and the angular velocity of the pendulum). This Kalman filter is implemented at each time step kT by propagating the following state estimation equation

$$\hat{\mathbf{x}}[(k+1)T] = \Phi\hat{\mathbf{x}}[kT] + \Theta u[kT] + L(y[kT] - C\hat{\mathbf{x}}[kT]), \tag{10}$$

where $L \triangleq (\Phi QC^{\rm T})(CQC^{\rm T} + V_2)^{-1}$ is the Kalman gain, V_2 is the measurement noise covariance matrix, and Q is obtained by solving the discrete-time algebraic Riccati equation [17]

$$Q = \Phi Q\Phi^{\rm T} + V_1 - (\Phi QC^{\rm T})(V_2 + CQC^{\rm T})^{-1}(\Phi QC^{\rm T})^{\rm T}, \tag{11}$$

where V_1 is the process noise covariance. Noise covariances are selected to be $V_1 = I_4$ and $V_2 = {\rm diag}(0.001, 0.001)$ to achieve acceptable closed-loop performance .

D. Controller Design

A linear quadratic regulator is designed such that the deviation of the pendulum angle is penalized heavily and the maximum allowable control effort is applied to the cart motor. The digital full-state feedback control law $u[kT] = -K_c\hat{\mathbf{x}}[kT]$ is used, where K_c is the control gain and $\hat{\mathbf{x}}[kT]$ is the state estimate returned from the Kalman filter. A linear quadratic approach is applied to design K_c so that the following quadratic cost function $J(u)$ is minimized

$$J(u) = \sum_{k=1}^{\infty}(\mathbf{x}^{\rm T}[kT]R_1\mathbf{x}[kT] + u^{\rm T}[kT]R_2u[kT]), \tag{12}$$

where R_1 is nonnegative-definite and R_2 is positive-definite. The control gain K_c is obtained from $K_c \triangleq (\Theta^{\rm T}P\Theta + R_2)^{-1}(\Theta^{\rm T}P\Phi)$, where P is the solution to the discrete-time algebraic Riccati equation [17]

$$P = \Phi^{\rm T}P\Phi + R_1 - (\Theta^{\rm T}P\Phi)^{\rm T}(\Theta^{\rm T}P\Theta + R_2)^{-1}(\Theta^{\rm T}P\Phi). \tag{13}$$

To give the controller priority over regulating pendulum angle, the state weighting matrix $R_1 = {\rm diag}(0.25, 10, 0, 0)$ is a diagonal matrix with the element corresponding to proportional control of pendulum angle larger than the other elements. The control weighting matrix $R_2 = 0.0003$ is set so that computed control actions are within the allowable voltage range of the cart motor.

V. Experimental Results

The IPC system is a nonlinear, high-bandwidth, open-loop unstable, underactuated plant. For such a system, the frame rate, image processing time, image resolution, and noise characteristics associated with measurements are critical factors to achieve closed-loop stability and acceptable performance of the wireless, vision-based feedback control. To investigate the potential of the proposed mounted smartphone approach for controlling the IPC test-bed, a series of experiments are performed to obtain insight into the relationships between these critical factors. See [12] for an illustrative video of the experiment.

A. Frame Rate, Computation Time, and Image Resolution

With vision-based measurements wirelessly transmitted from the smartphone to the PC at a fixed sampling rate, frame rate of the smartphone camera has an important impact on the closed-loop stability and performance of the system. Increases in frame rate are usually possible when using lower resolution camera presets. The iPhone 6 Plus supports frame rates up to 60 fps. Although image processing time does not affect the rate at which data arrives at the PC from the smartphone, this time represents the delay between the moment the visual data is relevant (the moment the frame is captured by the device camera) and the moment the data is received by the PC. With a frame rate of 60 fps, computation times of 0 to 16.667 ms are acceptable, however the larger computation times may cause noticeable effects on the stability of the closed-loop system. If the processing time of a single frame exceeds the amount of time allotted per frame, the subsequent frames are discarded until the processing of the current frame is completed. When frames are discarded, information about the state of the system is lost, and consistency in data collection rate is jeopardized, which has a significant impact on the stability of the closed-loop. To characterize the effects of different image resolutions on the computation time, frames are first captured at 10 Hz to avoid potentially discarding any frames. Table II shows the computation times obtained for a variety of image resolutions. After performing an experiment in which 200 measurements are collected from frames with a resolution of 192×144 pixels (the lowest resolution supported by the iPhone 6 Plus), the mean computation time is 5.09 ms with a standard deviation of 0.3609 ms, which is fast enough to support a 60 Hz frame rate from the device camera. Therefore, this resolution is chosen for the stabilization of the IPC (i.e., sampling time $T = 1/60$ second).

B. Measurement Noise

Although lower resolution presets allow for improvements in computation time, which must be fast enough to support the requirements set by the frame rate, lower resolution frames result in vision-based measurements with increased noise. This noise may jeopardize the stability and performance of the closed-loop system. Thus, to investigate the noise characteristics of the vision-based measurements at the chosen image resolution, raw data is obtained from the smartphone as it is mounted to the test-bed while it is kept still at its stable equilibrium configuration. This sensor data is collected and plotted as shown in Figure 6. Over the course of 20 second, the standard deviations of the cart position and pendulum angle measurements are 0.0258 cm and 0.1102°, respectively. Table II shows the amount of noise measured for a variety of image resolutions.

C. Sensor Validation

To assess the feasibility of using the vision-based measurements from the mounted smartphone, two additional tests are conducted to compare the accuracy and noise of the vision-based measurements to measurements obtained from

TABLE II: Effect of image resolution on computation time and measurement noise.

Image Resolution	Mean Computation Time (ms)	Computation Time SD (ms)	Cart Position SD (cm)	Pendulum Angle SD (°)
192×144	5.09	0.3609	0.0258	0.1102
640×480	16.4301	0.5546	0.0112	0.0391
1280×720	39.7369	1.3213	0.0056	0.0194

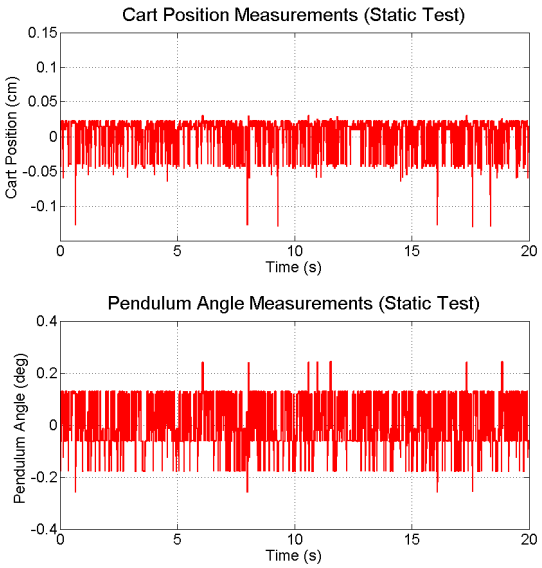

Fig. 6: Noise data collected in a static test.

a potentiometer connected to the output shaft of the cart motor and a digital encoder connected to the rotational axis of the pendulum arm. The first test, called a ramp test, is used to examine the characteristics of the measurements of cart position by applying a ramp reference to the cart position for approximately 3 seconds. Figure 7 shows the measurements reported by both the smartphone and the potentiometer, and confirms that the smartphone can accurately measure the position of the cart, although smartphone measurement suffers from a time delay of approximately 30 ms. A second test, called a drop test, is run to investigate the characteristics of the measurements of pendulum angle by lifting the pendulum arm a small amount from its stable equilibrium point, and dropping the pendulum arm to allow it to swing to a stop. Figure 8 shows the measurements reported by both the smartphone and the digital encoder. As can be seen from the figure, the smartphone can also accurately measure the angle of the pendulum, although the measurement suffers from the same time delay as noted above.

D. Inverted Pendulum on Cart Control

To explore the effect on the closed-loop response of the proposed system, the IPC test-bed is first controlled using measurements from the standard potentiometer and encoder sensors on board the test-bed (see Figure 9). After 10.5 seconds, the source of the measurements is switched to the visual measurements provided by the mounted smartphone for approximately 10 seconds until measurements from the

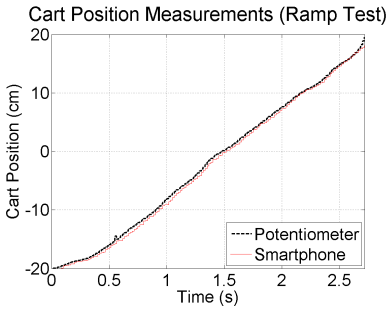

Fig. 7: Measurements of cart position from a ramp test.

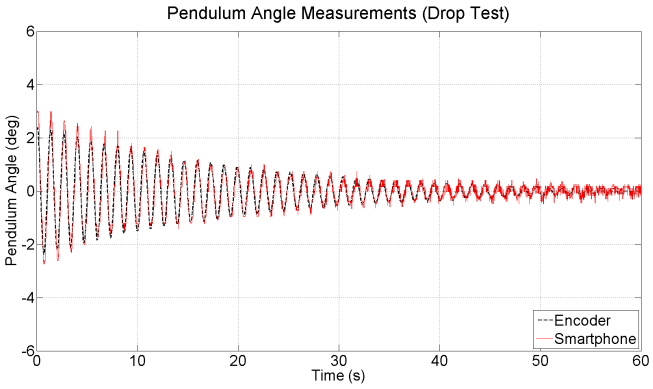

Fig. 8: Measurements of pendulum angle from a drop test.

potentiometer and encoder are selected again. Figure 9 shows the behavior of the cart position and pendulum angle before, during, and after the use of the vision-based measurements. The IPC system remains stable with the measurements from the mounted smartphone and exhibits a response comparable to that with measurements from the potentiometer and encoder sensors. The small variation between two responses can be attributed to small amount of communication delay, as well as an important trade-off between camera frame rate, image processing time, and image quality. With more robust computer vision techniques and mobile devices that can support superior image quality, faster frame rates, and faster computation, the performance of the IPC system with mounted smartphones can be improved further.

Note that while the pendulum and cart continue to exhibit small oscillations around the equilibrium state, the performance of the system with the vision-based measurements is indistinguishable from the performance with the test-bed's on-board potentiometer and encoder sensors. Thus, these oscillations are less likely to have resulted from measurement imprecision or communication delay, and are more likely due to imprecisely leveled test-bed and unmodeled phenomena like friction.

VI. Conclusion

This paper presents an approach that uses a mounted smartphone to perform vision-based control of an IPC test-bed. It is shown that the vision-based measurement and LQG-based control design methodology can render the IPC system stable. Future work will consider rule-based swing-up algorithms and markerless 3D pose estimation techniques executing on-board the smartphone. In addition, future research will investigate the effectiveness and user experience associated with the use of the proposed system in inquiry-based learning with the personal devices of students and researchers in classrooms and laboratories.

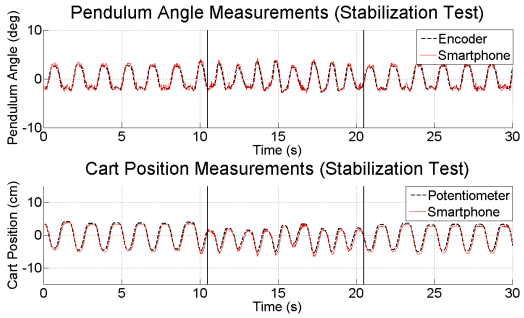

Fig. 9: Experimental results for the (a) cart position and (b) pendulum angle before, during, and after the use of vision-based measurements from the mounted smartphone.

References

[1] J. Apkarian, *A Comprehensive and Modular Laboratory for Control Systems Design and Implementation*. Quanser Consulting, 1995.

[2] D. L. Baggio, *Mastering OpenCV with Practical Computer Vision Projects*. Packt Publishing Ltd, Birmingham, UK, 2012.

[3] F. Chaumette and S. Hutchinson, "Visual servo control part II: Advanced approaches," *IEEE Robotics & Automation Magazine*, vol. 14, no. 1, pp. 109–118, 2007.

[4] E. S. Espinoza-Quesada and L. E. Ramos-Velasco, "Visual servoing for an inverted pendulum using a digital signal processor," in *IEEE Int. Symp. Signal Processing and Information Technology*, 2006, pp. 76–80.

[5] J. Frank and V. Kapila, "Development of mobile interfaces to interact with automatic control experiments [Focus on education]," *IEEE Control Systems*, vol. 34, no. 5, pp. 78–98, 2014.

[6] J. A. Frank, J. A. De Gracia Gomez, and V. Kapila, "Using tablets in the vision-based control of a ball and beam test-bed," in *Proc. Int. Conf. Informatics in Control, Automation, and Robotics*, Colmar, Alsace, France, 2015, pp. 92–102.

[7] N. R. Gans and S. A. Hutchinson, "Visual servo velocity and pose control of a wheeled inverted pendulum through partial-feedback linearization," in *IEEE/RSJ Int. Conf. Intelligent Robots and Systems*, 2006, pp. 3823–3828.

[8] S. Hutchinson, G. D. Hager, and P. I. Corke, "A tutorial on visual servo control," *IEEE Trans. Robotics and Automation*, vol. 12, no. 5, pp. 651–669, 1996.

[9] A. Kolker *et al.*, "Robot visual servoing using the example of the inverted pendulum," in *Int. Multi-Conf. Systems, Signals & Devices*, 2013, pp. 1–6.

[10] M. Monteiro, C. Cabeza, and A. C. Marti, "Rotational energy in a physical pendulum," *The Physics Teacher*, vol. 52, no. 3, pp. 180–181, 2014.

[11] M. Monteiro *et al.*, "Angular velocity and centripetal acceleration relationship," *The Physics Teacher*, vol. 52, no. 5, pp. 312–313, 2014.

[12] NYU. (2016) Visual Servoing of an Inverted Pendulum. [Online]. Available: http://engineering.nyu.edu/mechatronics/videos/invertedpendulum.html.

[13] K. Ogata, *Modern Control Engineering*. Prentice Hall, Upper Saddle River, NJ, 2009.

[14] R. Tapu *et al.*, "A smartphone-based obstacle detection and classification system for assisting visually impaired people," in *Int. Conf. Computer Vision Workshops*, 2013, pp. 444–451.

[15] H. Wang *et al.*, "Hybrid control for vision based cart-inverted pendulum system," in *American Control Conf.*, 2008, pp. 3845–3850.

[16] Z. Zhang, "A flexible new technique for camera calibration," *IEEE Trans. Pattern Analysis and Machine Intelligence*, vol. 22, no. 11, pp. 1330–1334, 2000.

[17] K. Zhou, J. C. Doyle, and K. Glover, *Robust and Optimal Control*. Prentice Hall, Englewood Cliffs, NJ, 1996.